Microfluid Nanofluid (2010) 9:41–53
DOI 10.1007/s10404-009-0518-2

RESEARCH PAPER

Incorporating ionic size in the transport equations for charged nanopores

Javier Cervera · Patricio Ramírez · José A. Manzanares · Salvador Mafé

Received: 2 August 2009 / Accepted: 21 September 2009 / Published online: 21 October 2009

Abstract Nanopores with fixed charges show ionic selectivity because of the high surface potential and the small pore radius. In this limit, the size of the ions could no longer be ignored because they occupy a significant fraction of the pore and, in addition, they would reach unrealistic concentrations at the surface if treated as point charges. However, most models of selectivity assume point ions and ignore this fact. Although this approach shows the essential qualitative trends of the problem, it is not strictly valid for high surface potentials and low nanopore radii, which is just the case where a high ionic selectivity should be expected. We consider the effect of ion size on the electrical double layer within a charged cylindrical nanopore using an extended Poisson–Boltzmann equation, paying special attention to (non-equilibrium) transport properties such as the streaming potential, the counter-ion transport number, and the electrical conductance. The first two quantities are related to the nanopore selectivity while the third one characterizes the conductive properties. We discuss the nanopore characteristics in terms of the ratio between the electrolyte and fixed charge concentrations and the ratio between the ionic and nanopore radii showing the experimental range where the point ion model can still be useful. Even for relatively small inorganic ions at intermediate concentrations, ion size effects could be significant for a quantitative estimation of the nanopore selectivity in the case of high surface charge densities.

J. Cervera · J. A. Manzanares · S. Mafé (✉)
Fac. de Física, Universitat de València, 46100 Burjassot, Spain
e-mail: smafe@uv.es

P. Ramírez
Depto. de Física Aplicada, Universidad Politécnica de Valencia, 46022 Valencia, Spain

Keywords Nanopores · Ion size · Poisson–Boltzmann equation · Ionic selectivity · Conductance

1 Introduction

The primary application of fixed charge nanopores is to provide ionic selectivity and sensing exploiting the fact that the pore size is not much larger than the ionic analyte size (Martin and Siwy 2007; Höltzel and Tallarek 2007; Griffiths 2008; Abgrall and Nguyen 2008; Schoch et al. 2008). Therefore, the question of the effect of the analyte size on the nanostructure performance naturally arises. In the Coulter counting method, for example, the analyte size is estimated from the increase in the resistance observed as it passes through a fluidic constriction separating two reservoirs (Petrossian et al. 2008). Resistive-pulse sensing allows for single-molecule mass spectrometry in solution using a nanopore (Lee et al. 2004; Robertson et al. 2007; Sexton et al. 2007a, b; Wharton et al. 2007; Griffiths 2008; Abgrall and Nguyen 2008). The principles of single-molecule sensing were suggested and analyzed in earlier papers (Kasianowicz et al. 1996 and references therein). The nanopore, however, does not act simply as a mechanical filter: it displays also ionic selectivity because of the electrical charges attached to the surface. In the case of electrolyte solutions with small inorganic ions, which is relevant to water desalination and biological membranes, these charges favor the passage of counter-ions (ions with charge opposite to that of the pore) but hinder the passage of co-ions (ions with charge of the same sign as the pore) (Siwy and Fulinski 2002; Jorne 2006; Cervera et al. 2006; Ali et al. 2009).

Nanopores with high surface charge density on the pore walls are likely to exhibit high ionic selectivity because

their (molar) concentration of fixed charges, which increases with increasing surface charge density and with decreasing pore radius, is larger than the external electrolyte concentration. It is well known that the diffuse double layer theory can give a suitable description of the ion and potential distributions only when the concentrations of fixed charges and mobile ions are low enough. At high surface charge densities, unrealistic counter-ion accumulation at the pore walls casts some doubts on the model predictions, and ion size effects should be included (Guzmán-García et al. 1990; Cwirko and Carbonell 1992; Bontha and Pintauro 1994; Basu and Sharma 1997). In the past, these effects have proved significant in problems of physical chemistry and biophysics including the ion distribution in the vicinity of a planar charged surface immersed in an electrolyte solution (Borukhov et al. 1997; Paunov and Binks 1999), the transport of ionic drugs across the paracellular pathway of cell monolayers (Pade and Stavchansky 1997), and the modeling of ionic transport through biological ion channels (natural nanotubes) (Eisenberg 1998).

Tables 1 and 2 illustrate the nature of the problem. Table 1 considers the ratio $(R_i/R_p)^2$, where R_i and R_p are the ionic and nanopore radii, respectively, for a wide range of experimental values. The ionic crystal radius (approximately 0.1 nm for small inorganic ions) is significantly smaller than the hydrated ion radius (approximately 0.3 nm). This radius is the relevant quantity in aqueous solutions because the small ions move together with a water layer: it is the effective hydrated radii that dictates the ion mobility in bulk solutions. Organic ions [e.g., those having the tetraalkylammonium structure, usually employed as ion channel blockers (Hille 2001)] have significantly larger radii (0.3–0.5 nm) while aromatic compounds (e.g., sodium benzene sulfonate) have longer molecular axis in the range 0.5–1 nm (Jin et al. 2005). Finally, macro-ions have characteristic lengths significantly higher than 1 nm (Karginov et al. 2005), with protein gyration and Stokes radii as high as 2–4 nm (Chun et al. 2006). The nanopore radii of Table 1 span also over a wide region of experimental values. Ion channels in biological membranes are usually <1–2-nm wide (Hille 2001) with some biological pores such as the bacterial outer membrane porin (OmpF) (Alcaraz et al. 2004, 2006) and the PA_{63} channels [involved in the anthrax infection (Karginov et al. 2005; Aguilella-Arzo et al. 2006)] having radii in the range 1–2 nm. These are close to those of the smaller synthetic nanopores (Dekker 2007; Tabard-Cossa et al. 2007; Healy et al. 2007; Zhao et al. 2007; Griffiths 2008) and carbon nanotube membranes (Yeh and Hummer 2004). Conical nanopores have tip and base radii in the ranges 1–10 nm and 100–500 nm (Siwy and Fulinski 2002; Spohr 2005; Cervera et al. 2006; Healy et al. 2007; Martin and Siwy 2007; Sexton et al. 2007b; Apel et al. 2007; Cornelius et al. 2007; Ramírez et al. 2008), respectively, while nanoporous membranes radii are typically 5–25 nm (Cwirko and Carbonell 1992; Nishizawa et al. 1995; Chun et al. 2006; Ku et al. 2007; Striemer et al. 2007). The results of Table 1 show clearly that inorganic and organic ions tend to occupy a significant fraction of the nanopore cross section, this trend being more pronounced for big organic ions and macro-ions, where the size effect is dominant in most applications (Sexton et al. 2007a, b; Wharton et al. 2007; Healy et al. 2007; Zhao et al. 2007; Striemer et al. 2007). The numbers in italics approximately indicate the region, where size effects are expected to be significant (note that some of them are limiting cases not achieved in practice).

Table 1 emphasizes only the *geometrical* problem. To better understand the *electrochemical* consequences of treating ions as point charges, Table 2 shows the surface counter-ion concentrations that would result from using a Gouy–Chapman approach for the radial distribution of the ionic concentration in the pore. In this approach, the concentration at the center of the pore (which is the bulk solution concentration approximately) and the concentration at the pore surface are related by the Boltzmann factor $\exp(F\phi^{surface}/RT)$ where $\phi^{surface}$ is the surface potential, R is the gas constant, T is the temperature, and F is the Faraday

Table 1 The ratio $(R_i/R_p)^2$ (in %) where R_i and R_p are the ion and nanopore radii, respectively, is a measure of the nanopore cross section occupied by the (finite size) ionic permeant

$(R_i/R_p)^2$ (%)				
R_i (nm)	0.1 (crystal radius of inorganic ion)	0.3 (effective radius of hydrated inorganic ion)	0.5 (organic ion/ aromatic compound)	1 (macro-ion)
$R_p = 1$ nm (ion channel)	1	*9*	*25*	*100*
$R_p = 2$ nm (wide ion channel/ carbon nanotube/tip of conical nanopore)	0.25	*2*	*6*	*25*
$R_p = 3$ nm (nanopore)	0.1	1	*3*	*10*
$R_p = 5$ nm (nanoporous membrane)	0.04	0.4	1	*4*

The numbers in italics approximately indicate the region where size effects are expected to be significant

Table 2 The counter-ion concentration at the pore surface, $c^{surface}$, obtained using a Gouy–Chapman approach for the ionic radial distribution, as a function of the surface potential, $\phi^{surface}$

$c^{surface}$ (M)						
$\phi^{surface}$ (mV)	10	25	50	100	125	150
$c_s = 0.01$ M	0.015	0.03	0.07	0.50	1.3	*3.4*
$c_s = 0.1$ M	0.15	0.3	0.7	*5*	*13*	*34*
$c_s = 1$ M	1.5	*3*	*7*	*50*	*130*	*340*

The numbers in italics approximately indicate the region where the accumulation of (point) ions is likely to be unrealistic

constant. The numbers in italics approximately indicate the region, where the accumulation of (point) ions is likely to be unrealistic and could lead to misleading conclusions. The results of Table 2 show that the size effect is already significant at moderately high surface potentials and electrolyte concentrations. We propose to study here this question using a generalized Poisson–Boltzmann (P–B) equation, showing the experimental region where the ionic size can be safely ignored, and discussing the size effects on the selectivity and transport in the nanopore.

Despite the nanometer scales involved, the fact is that most models of selectivity are still based on the classical continuum theories because these are relatively simple and predict correctly the qualitative trends of the problem (Siwy and Fulinski 2002; Lee et al. 2004; Cervera et al. 2006; Jorne 2006; Aguilella-Arzo et al. 2006; Ramírez et al. 2003a, 2007, 2008; Vlassiouk and Siwy 2007; Gracheva et al. 2007). Some approaches consider the linearized P–B equation for point ions (Schoch et al. 2008; Jorne 2006, Aguilella-Arzo et al. 2006). In those cases where the exact, nonlinear P–B equation is employed, ion size effects are usually ignored (Westermann-Clark and Christoforou 1986; Cervera et al. 2006; Aguilella-Arzo et al. 2006; Vlassiouk and Siwy 2007) despite the fact that the electrolyte solution is confined to the reduced free space available within the nanopore. Studies of the nanopore selectivity using a generalized P–B equation that incorporates explicitly the size of the ions (Bontha and Pintauro 1994; Basu and Sharma 1997; Cervera et al. 2003) are lacking. These would be of great interest to doped-semiconductor membranes (Gracheva et al. 2007), nanotubule membranes (Nishizawa et al. 1995; Ramírez et al. 2003a; Chun et al. 2006; Ku et al. 2007), nanofluidic channels and nanoslits (Stein et al. 2004; Schoch et al. 2008) conical nanopores (Siwy and Fulinski 2002; Lee et al. 2004; Cervera et al. 2006; Ramírez et al. 2007, 2008), nanopipettes (Umehara et al. 2006), nanocables (Lebedev et al. 2005), nanochannel-based fuel cells (Liu et al. 2005), nanoelectrodes (Zhang et al. 2006), and the ion channels of biological membranes (Hille 2001; Karginov et al. 2005; Alcaraz et al. 2006; Aguilella-Arzo et al. 2006; Miedema et al. 2007).

The P–B approach for the ionic radial distribution in the nanopore considers the ions as point charges and the water as a dielectric continuum, despite the fact that atomistic details should be significant as the nanopore radius becomes comparable to the ionic radius. Atomistic simulations, in particular the Molecular Dynamics (Qiao and Aluru 2005) and Monte Carlo (Hou et al. 2008) methods, are increasingly used to study nanometer wide channels, but they require considerable numerical effort and do not provide intuitive equations to understand the basic transport phenomena, contrary to the case of the continuum approaches (Cwirko and Carbonell 1992; Siwy and Fulinski 2002; Lee et al. 2004; Yeh and Hummer 2004; Heins et al. 2005; Aguilella-Arzo et al. 2006; Muthukumar and Kong 2006). While molecular simulations are more rigorous than the P–B equation for the length scales involved, the fact is that extensions of this approach have often proved useful (Guzmán-García et al. 1990; Bontha and Pintauro 1994; Cervera et al. 2003) because long-range electrostatic forces rather than atomistic-level details dominate the behavior of macroscopic transport phenomena (Eisenberg 1998; Siwy and Fulinski 2002; Lee et al. 2004; Cervera et al. 2006; Ramírez et al. 2008). Therefore, an intermediate, useful approach is to generalize the P–B approach to incorporate either explicitly (Cervera et al. 2003) or implicitly (García-Morales and Mafé 2007) the ion size effects. This leads to new intuitive physical results and allows us to discuss the qualitative trends of ions size effects while keeping the numerical complexity to a minimum.

Modifications of the P–B equation which incorporate the volume of the hydrated ions have been proposed by Bikerman (1942), Grimley and Mott (1947), Freise (1952), Wicke and Eigen (1953), Brodowsky and Strehlow (1959), Levine and Bell (1960), and Sparnaay (1972). These studies have evidenced the difficulties involved in an accurate statistical description of electrolyte solutions at high concentrations. Nevertheless, most of these modifications of the P–B equation appear to be correct at least for moderate concentrations (of the order of 0.1 M for a 1:1 electrolyte).

The present work goes one step further by including the size effects in the modified P–B equation, the diffusion coefficients (Renkin 1954), and the transport equations (Cervera et al. 2003), as suggested in the fundamental contributions by Haase (1969) and Buck (1984). The physical model is based on the Nernst–Planck equations to describe the flux of the ionic species, the Navier–Stokes equation to obtain the solution velocity inside the pore, and an extended P–B equation to calculate the radial distribution of the electrical potential and ionic concentrations. Although some authors have proposed more complicated structures, particularly for Nafion membranes (Haubold

et al. 2001), in this work the nanopore is considered as a cylinder with charged wall, as is usual in these space–charge models. Because we wish to study the ion size effects on the (non-equilibrium) transport properties such as the streaming potential, counter-ion transport number (selectivity), and electrical conductance, we will focus on the case of a symmetric electrolyte solution. Generalizing our approach to the case of ions with charge and size asymmetries (Hou et al. 2008) would allow describing additional effects such as adsorption and charge inversion at the nanopore surface as well as other specific water–ion interactions.

This work is organized according to the following scheme. First, we describe the steady-state transport equations and the incorporation of finite size effects in the ionic activity and the osmotic pressure. In particular, we analyze how the P–B equation is generalized to incorporate the ion size. The equations are formally integrated using a pore-averaging technique which leads to simple equations for the conductance G, the counter-ion transport number t_+, and the streaming potential v. Then, the numerical solution of the generalized P–B equation is used to evaluate the average ionic concentrations, which are necessary to understand the macroscopic transport phenomena, and the transport properties G, t_+, and v as functions of experimental parameters such as the electrolyte concentration, the surface charge density and the ratio between the ionic and the pore radii. The contribution of the electro-osmotic flow to these transport properties is analyzed in detail because the finite size of the ions can enhance the importance of convection as a transport mechanism.

2 Theoretical modeling

We consider a single cylindrical nanopore immersed in a 1:1 electrolyte of molar concentration c_s, as shown in Fig. 1. The pore fixed charges are modeled as a uniform surface charge density $\sigma < 0$. The Nernst–Planck equation for the ionic flux density in the nanopore-fixed reference frame is

$$\vec{j}_i = \vec{u}c_i - D_i c_i \nabla[\ln a_i + z_i f\phi], \tag{1}$$

where D_i and z_i are the diffusion coefficient and the charge number of species i, respectively, and $f \equiv F/RT$. The solution velocity $\vec{u}$ is obtained from the Navier–Stokes equation

$$\eta\nabla^2\vec{u} = \nabla p + \rho_e\nabla\phi, \tag{2}$$

where $\rho_e = F(c_+ - c_-)$ is the electrical charge density, η is the solution viscosity, and p is the pressure. Finally, the electric potential ϕ is determined by the Poisson equation

$$\nabla^2\phi = -\frac{\rho_e}{\varepsilon}, \tag{3}$$

where ε is the electrical permittivity. Equations 1–3 describe the ion transport through the nanopore. The size effect can be described through the activity of ionic species i (Cervera et al. 2003)

$$a_i = \frac{c_i}{1 - v\sum_k c_k}, \tag{4}$$

where v is the partial molar volume of the ions assumed to be equal for the two ionic species.

Since the nanopore length L (which is of the order of micrometers) is much higher than the nanopore radius R_p (which is of the order of nanometers), we can assume that $\vec{j}_i$ and $\vec{u}$ have only axial components denoted by j_i and u. The continuity equations $\partial j_i/\partial x = 0$ and $\partial u/\partial x = 0$ then require that these quantities are functions of the radial position coordinate only, $j_i = j_i(r)$ and $u = u(r)$. Introducing the electrostatic potential

$$\psi(r,x) \equiv -\frac{1}{z_i f}\ln\frac{a_i}{a_\pm} \tag{5}$$

the equilibrium condition for the radial ionic distribution (radial component of Eq. 1)

$$\frac{\partial}{\partial r}[\ln a_i + z_i f\phi] = 0 \tag{6}$$

implies that the electrolyte mean activity

$$a_\pm(x) \equiv [a_+(r,x)a_-(r,x)]^{1/2} \tag{7}$$

and the electromotive potential

$$V(x) \equiv \phi(r,x) - \psi(r,x) \tag{8}$$

are functions of the axial position x only. Similarly, the mechanical equilibrium condition (radial component of Eq. 2)

$$\frac{\partial p}{\partial r} + \rho_e\frac{\partial\phi}{\partial r} = \frac{\partial}{\partial r}(p - \Pi) = 0 \tag{9}$$

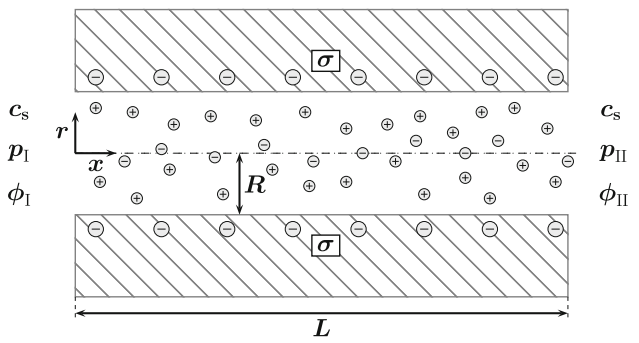

Fig. 1 Schematic view of a negatively charged nanopore separating two 1:1 electrolyte solutions (I and II) of the same concentration c_s at different electric potentials (ϕ_I and ϕ_{II}) and pressures (p_I and p_{II})

implies that the so-called solvent pressure

$$P(x) \equiv p(r,x) - \Pi(r,x) \tag{10}$$

is a function of x only. The last equality in Eq. 9 has been obtained from Eq. 6 and the Bjerrum relation for the osmotic pressure, $\mathrm{d}\Pi = RT\sum_k c_k \mathrm{d}\ln a_k$. This latter relation can be integrated to

$$\Pi = -\frac{RT}{v}\ln\left(1 - v\sum_k c_k\right), \tag{11}$$

which reduces to the classical expression $\Pi^0 = RT\sum_k c_k$ in the case of point ions ($v \to 0$).

In terms of variables $a_\pm$, V, and P, the transport Eqs. 1 and 2 can be presented as

$$j_i = uc_i - D_i c_i\left(\frac{\mathrm{d}\ln a_\pm}{\mathrm{d}x} + z_i f\frac{\mathrm{d}V}{\mathrm{d}x}\right) \tag{12}$$

$$\eta\frac{1}{r}\frac{\partial}{\partial r}\left(r\frac{\partial u}{\partial r}\right) = \frac{\mathrm{d}P}{\mathrm{d}x} + \rho_\mathrm{e}\frac{\mathrm{d}V}{\mathrm{d}x} \tag{13}$$

The variables $a_\pm$, V, and P are defined inside the nanopore. They are related to c, ϕ, and p in the external solutions by the boundary conditions that specify the transport and mechanical equilibria between the external (I and II) and internal solutions at the nanopore ends ($x = 0$ and L)

$$a_\pm(0) = a_\pm(L) = a_\mathrm{s} = \frac{c_\mathrm{s}}{1 - 2vc_\mathrm{s}} \tag{14}$$

$$V(0) = \phi_\mathrm{I}; \quad V(L) = \phi_\mathrm{II} \tag{15}$$

$$P(0) = p_\mathrm{I} - \Pi_\mathrm{s}; \quad P(L) = p_\mathrm{II} - \Pi_\mathrm{s} \tag{16}$$

Thus, the axial gradients are $\mathrm{d}P/\mathrm{d}x = -\Delta p/L = (p_\mathrm{II} - p_\mathrm{I})/L$, $\mathrm{d}V/\mathrm{d}x = -\Delta V/L = (\phi_\mathrm{II} - \phi_\mathrm{I})/L$, and $\mathrm{d}\ln a_\pm/\mathrm{d}x = 0$ because the two external solutions have the same electrolyte concentration (and the same osmotic pressure $\Pi_\mathrm{s} = 2RTc_\mathrm{s}$) in the system under consideration.

From Eqs. 4, 5 and 14, the radial distribution of the ionic concentration is determined by the electrostatic potential ψ through the Bikerman equation (Bikerman 1942)

$$c_i = \frac{1 - v\sum_k c_k}{1 - 2vc_\mathrm{s}} c_\mathrm{s}\exp(-z_i f\psi), \tag{17}$$

which can also be presented as $a_i = a_\mathrm{s}\exp(-z_i f\psi)$ and is a generalization of the Boltzmann relation $c_i = c_\mathrm{s}\exp(-z_i f\psi)$ that incorporates the finite size of the ions. From Eq. 17, the total ionic concentration inside the nanopore is

$$c_+ + c_- = \frac{2c_\mathrm{s}\cosh(f\psi)}{1 + 2vc_\mathrm{s}[\cosh(f\psi) - 1]} \tag{18}$$

and the P–B equation can be generalized to

$$\frac{1}{r}\frac{\partial}{\partial r}\left(r\frac{\partial\psi}{\partial r}\right) \approx -\frac{\rho_\mathrm{e}}{\varepsilon} = \frac{\kappa_{D,\mathrm{s}}^2}{f}\frac{\sinh(f\psi)}{1 + 2vc_\mathrm{s}[\cosh(f\psi) - 1]} \tag{19}$$

where $\kappa_{D,\mathrm{s}} \equiv [2F^2c_\mathrm{s}/\varepsilon RT]^{1/2}$ is the reciprocal Debye length referred to the external solution, and the term $\partial^2\phi/\partial x^2$ in the Poisson equation has been neglected because $L \gg R_\mathrm{p}$. Note that Eq. 18 imposes bounds to the total ionic concentration, $2c_\mathrm{s} \le c_+ + c_- \le 1/v$, and therefore it avoids the unrealistic values sometimes found when considering point ions. Equation 19 is subject to the boundary conditions

$$\left.\frac{\partial\psi}{\partial r}\right|_{r=0} = 0, \tag{20}$$

which follows from the cylindrical symmetry, and the Gauss law

$$\left.\frac{\partial\psi}{\partial r}\right|_{r=R_\mathrm{p}-R_\mathrm{i}} = \frac{\sigma}{\varepsilon}\frac{R_\mathrm{p}}{R_\mathrm{p} - R_\mathrm{i}} \tag{21}$$

that can be derived from the electroneutrality condition in the nanopore cross section and the fact that no charge is present in the region $R_\mathrm{p} - R_\mathrm{i} < r < R_\mathrm{p}$ (Mafé et al. 1990). From Eqs. 19 to 21, we conclude that the electrostatic potential ψ defined in Eq. 5 is the contribution to ϕ that describes the interaction between the ions and the fixed charges at the nanopore surface.

Using Eq. 19, the Navier–Stokes equation (Eq. 13) can be formally integrated with the non-slip condition $u = 0$ at $r = R_\mathrm{p} - R_\mathrm{i}$ to yield the solution velocity

$$u(r) = \frac{(R_\mathrm{p} - R_\mathrm{i})^2 - r^2}{4\eta}\frac{\Delta p}{L} + \frac{\varepsilon}{\eta}[\psi(r) - \psi^\mathrm{s}]\frac{\Delta V}{L}, \tag{22}$$

where $\psi^\mathrm{s} \equiv \psi(R_\mathrm{p} - R_\mathrm{i})$ is the surface electrostatic potential (i.e., the electrostatic potential at the position of closest approach of the ions to the pore wall). Equation 22 shows that there is convection even in the absence of a pressure difference between the external solutions. The last term in Eq. 22 accounts for the electro-osmotic flow which originates from the electrical force that acts on the charged pore solution.

Defining the average of a function $f(r)$ over the pore cross section as

$$\langle f\rangle \equiv \frac{2}{R_\mathrm{p}^2}\int_0^{R_\mathrm{p}-R_\mathrm{i}} f(r)r\mathrm{d}r \tag{23}$$

the average flux density of species i is obtained from Eq. 12 as

$$\langle j_i\rangle = \langle uc_i\rangle - \frac{1}{z_i F}\langle\kappa_i\rangle\frac{\mathrm{d}V}{\mathrm{d}x} \tag{24}$$

In the absence of applied pressure difference, Eq. 22 leads to

$$\langle j_i\rangle|_{\Delta p=0} = -\frac{1}{z_i F}\langle\kappa_i + \kappa_{c,i}\rangle\frac{\mathrm{d}V}{\mathrm{d}x}, \tag{25}$$

where $\kappa_i \equiv F^2 D_i c_i/RT$ and $\kappa_{c,i} \equiv (F\varepsilon/\eta) z_i c_i [\psi(r) - \psi^s]$ are the migrational and convective contributions of species i to the electrical conductivity (Kontturi et al. 2008). The electrical conductance is

$$G \equiv \left.\frac{I}{\Delta V}\right|_{\Delta p=0} = \frac{\pi R_p^2}{L}\langle \kappa + \kappa_c \rangle, \tag{26}$$

where $I = \pi R_p^2 F \langle j_+ - j_- \rangle$ is the electric current and $\kappa = \kappa_+ + \kappa_-$ and $\kappa_c = \kappa_{c,+} + \kappa_{c,-}$ are the migrational and convective electrical conductivities, respectively. The (integral) counter-ion transport number is

$$t_+ \equiv \left.\frac{\pi R_p^2 F \langle j_+ \rangle}{I}\right|_{\Delta p=0} = \frac{\langle \kappa_+ + \kappa_{c,+} \rangle}{\langle \kappa + \kappa_c \rangle}. \tag{27}$$

An applied pressure difference Δp generates a hydraulic flow of solution across the nanopore (see Eq. 22). Because the pore solution bears an electrical charge density $\rho_e > 0$ whose average value is $\langle \rho_e \rangle = FX = -2\sigma/R_p$, this hydraulic flow produces a charge separation which eventually creates a potential difference ΔV. The ratio of ΔV to Δp under zero current conditions, $\langle j_+ \rangle = \langle j_- \rangle$, is the streaming potential v and can be evaluated from Eq. 24 as

$$v \equiv \left.\frac{\Delta V}{\Delta p}\right|_{I=0} = \frac{1}{4\eta}\frac{\langle r^2 \rho_e \rangle - (R_p - R_i)^2 FX}{\langle \kappa + \kappa_c \rangle} \tag{28}$$

3 Results and discussion

The following results have been obtained for a nanopore of radius R_p = 3 nm and length L = 10 μm. For the surface charge density, we have considered the values $\sigma = -0.1$ and -0.5 e/nm^2, which are equivalent to fixed charge concentrations $X \equiv -2\sigma/FR_p = 0.11$ and 0.55 M. These values are typical of nanopores (Westermann-Clark and Christoforou 1986; Apel and Pretzsch 1986; Manzanares et al. 1991; Ramírez et al. 2003b; Chun et al. 2006; Ku et al. 2007). The external electrolyte concentrations have been assigned values between 0 and 0.8 M. The radii ratio R_i/R_p assumes values ranging from 0 (point ions) to 0.1 (R_i = 0.3 nm). We estimate the partial molar volume of the ions as $v = N_{Av}(4\pi/3)(2R_i)^3$, where N_{Av} is Avogadro's number. This expression follows from statistical mechanics arguments by considering the ionic solution as a gas of hard spheres (Paunov and Binks 1999). The ionic radius R_i = 0.3 nm corresponds to a volume fraction occupied by the ions of $2vc_s = 0.11$ when c_s = 0.1 M. The radii ratio R_i/R_p also affects the diffusion coefficient of the ions inside the nanopore. This effect is accounted for the Renkin equation

$$D_i = D_i^0 \left[1 - 2.104\frac{R_i}{R_p} + 2.09\left(\frac{R_i}{R_p}\right)^3 - 0.95\left(\frac{R_i}{R_p}\right)^5\right], \tag{29}$$

where D_i^0 is the ionic diffusion coefficient in the (free) aqueous solution. The Renkin equation is valid for $R_i/R_p \le 0.4$ (Renkin 1954). The free diffusion coefficients have the values $D_+^0 = D_-^0 = 2 \times 10^{-5}$ cm^2/s, which correspond to K^+ and Cl^- ions approximately. Other parameters are T = 300 K, η = 1 mPa s, and $\varepsilon = 80\varepsilon_0$, where ε_0 is the vacuum permittivity.

3.1 Average ionic concentrations

Most transport properties of charged nanopores are significantly influenced by the ionic concentrations in their interior. Their values result from the interplay of three dimensionless parameters: (i) the ratio X/c_s between the fixed charge concentration and the external electrolyte concentration, (ii) the ratio $\kappa_{D,X}R_p$ between the nanopore radius and the Debye length $1/\kappa_{D,X} \equiv [\varepsilon RT/F^2 X]^{1/2}$ referred to the fixed charge, and (iii) the volume fraction $2vc_s$ occupied by the ions in the external solution, which accounts for the finite ion size. In the classical Donnan theory, the co-ion concentration inside the nanopore is

$$c_{-,D} = \left[(X/2)^2 + c_s^2\right]^{1/2} - X/2 \tag{30}$$

so that $\sinh[\ln(c_{-,D}/c_s)] = -X/2c_s$. In our theoretical modelling the ratio X/c_s determines the average value

$$\frac{\langle \rho_e \rangle}{2Fc_s} = -\left\langle \frac{\sinh(f\psi)}{1 + 2vc_s[\cosh(f\psi) - 1]} \right\rangle = \frac{\kappa_{D,X}^2}{\kappa_{D,s}^2} = \frac{X}{2c_s} \tag{31}$$

that is, it roughly determines the average value of the electrostatic potential. The differences between these two equations are that Eq. 31 is valid for finite size ions and accounts for the existence of a radial electrical double layer while Eq. 30 is valid for point ions and assumes that the electrostatic potential is uniform (in the radial direction). Otherwise, these equations are similar and therefore the ratio X/c_s is an important factor in determining the average ionic concentrations inside the nanopore. The ratio $\kappa_{D,X}R_p$ determines the electric field at the pore surface

$$\left.\left(r\frac{\partial \psi}{\partial r}\right)\right|_{r=R_p-R_i} = -\frac{\kappa_{D,X}^2 R_p^2}{2f} \tag{32}$$

and hence the importance of radial electrical double layer in the electrokinetic effects. If $\kappa_{D,X}R_p << 1$ (for which R_p = 3 nm means $-\sigma << 0.02$ e/nm^2) the radial profile of the electrostatic potential is nearly flat and the classical Donnan theory provides a good estimate of the average co-ion concentration inside the nanopore in the case of point ions. On the contrary, in the case $\kappa_{D,X}R_p \gg 1$ that we consider in the calculations, the electrostatic potential has a large variation in the radial direction and, in the

case of point ions, the average co-ion concentration inside the nanopore is larger than predicted by Eq. 30 (Kontturi et al. 2008). This effect is particularly noticeable when $c_s < X$, otherwise the radial electrical double layer is restricted to the close vicinity of the pore wall and a large fraction of the nanopore cross section is practically electroneutral.

It is intuitive that the ionic concentrations inside the nanopore must be lower for finite size than for point ions, under the same conditions, because of the increased osmotic pressure $\Pi \geq \Pi^0$, and this must also hold true for their average values $\langle c_+ \rangle$ and $\langle c_- \rangle$. Since the average value of the charge density $\rho_e = F(c_+ - c_-)$ inside the pore is determined by the electroneutrality condition in the pore cross section $\langle c_+ \rangle - \langle c_- \rangle = X = -2\sigma/FR_p$, increasing the ion size does not affect the difference $\langle c_+ \rangle - \langle c_- \rangle$, but decreases both $\langle c_+ \rangle$ and $\langle c_- \rangle$. In other words, co-ion exclusion is enhanced by finite ion size effects. This explains the superior selectivity of nanopores compared to larger pores for the same values of X and c_s. In order to prove that the ionic concentrations inside the nanopore are lower for finite size than for point ions, we can write Eq. 17 as $c_+c_- = (\gamma_s^2/\gamma_+\gamma_-)c_s^2$, where $\gamma_i \equiv 1/\left(1 - \nu \sum_k c_k\right)$ is the activity coefficient of species i. At any position inside the nanopore the total ionic concentration is larger than in the external solution, $c_+ + c_- \geq 2c_s$. This is a well-known consequence of the existence of a radial electrical double layer in the case of point ions (Kontturi et al. 2008) and it can also be deduced from Eq. 18 in the case of finite size ions because the volume fraction occupied by the ions is lower than one, $2\nu c_s < 1$. Then, the activity coefficient γ_i is larger inside the nanopore than in the external solution, $\gamma_+\gamma_- \geq \gamma_s^2$, and therefore $c_+c_- \leq c_s^2$ where the equal sign only holds for point ions.

Figure 2a, b illustrates that the average co-ion concentration $\langle c_- \rangle$ in a nanopore deviates from the value $c_{-,D}$ predicted by the classical Donnan theory, Eq. 30. Since $\langle c_+ \rangle = \langle c_- \rangle + X$, the counter-ion concentration shows the same absolute deviation from Donnan theory. These figures show $\langle c_- \rangle / c_{-,D}$ versus the external electrolyte concentration for point ions and finite-size ions with $R_i = 0.1$, 0.2, and 0.3 nm; recall that $\langle c_+ \rangle = \langle c_- \rangle + X$. As explained above, $\langle c_- \rangle / c_{-,D} > 1$ in the case of point ions because of the radial variation of the electrostatic potential. This effect is more noticeable in the case of a highly charged nanopore illustrated in Fig. 2a. Increasing ion size decreases the average concentration, and hence enhances the co-ion exclusion. For the larger finite-size ions here considered ($R_i = 0.3$ nm) the average concentrations is below that predicted by the classical Donnan theory, and this effect is more noticeable in the case of a weakly charged nanopore illustrated in Fig. 2b.

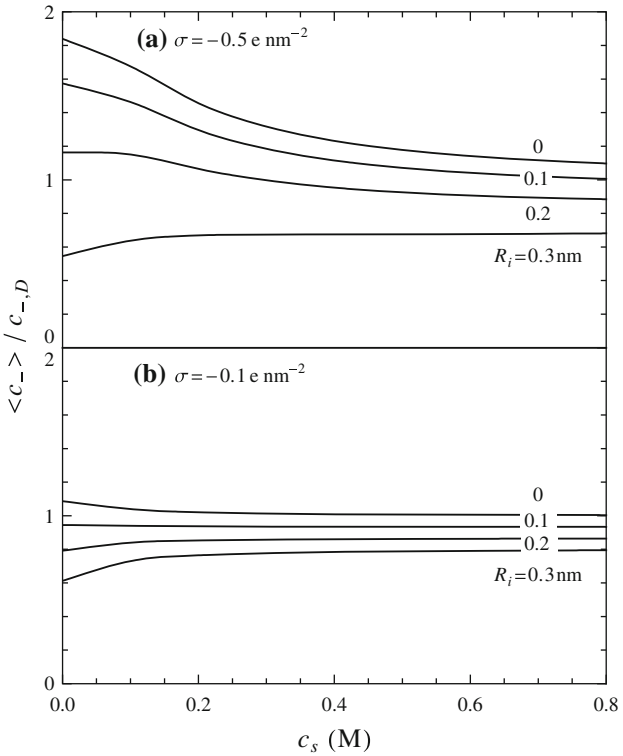

Fig. 2 Average co-ion concentration relative to the value $c_{-,D}$ predicted by the classical Donnan theory, $\langle c_- \rangle / c_{-,D}$ versus the external electrolyte concentration for point and finite-size ions with $R_i = 0.1$, 0.2, and 0.3 nm. The nanopore surface charge density is **a** $\sigma = -0.5$ e/nm^2 and **b** $\sigma = -0.1$ e/nm^2

3.2 Electrical conductance

Figure 3a, b shows the nanopore electrical conductance as a function of the external electrolyte concentration for the cases of point and finite size ions at different values of the surface charge density. The migrational contribution to the average electrical conductivity, $\langle \kappa \rangle \equiv F^2 D_i \langle c_+ + c_- \rangle / RT$, is simply proportional to the average ionic concentrations and therefore can be understood from Figs. 2a, b. In the classical Donnan theory $c_{+,D} + c_{-,D} = \sqrt{X^2 + 4c_s^2}$ and, therefore, $\langle \kappa \rangle$ increases with c_s (at constant X or σ) as $\sqrt{X^2 + 4c_s^2}$, which saturates at low c_s and shows a linear increase at high c_s. Basically, this is the behavior observed in Fig. 3a, b. Since finite size ions have values of $\langle c_+ + c_- \rangle$ lower than point ions, the migrational conductivity must decrease with increasing ionic radius. Moreover, the Renkin correction factor $D_i/D_i^0 \leq 1$, which accounts for the reduced mobility of finite size ions in nanopores, also leads to a 20% reduction in the migrational conductivity when $R_i/R_p = 0.1$.

The presence of electric charges on the pore walls implies that there is volume flow, even in the absence of a pressure difference between the external solutions. This electro-osmotic flow arises from the electrical force that

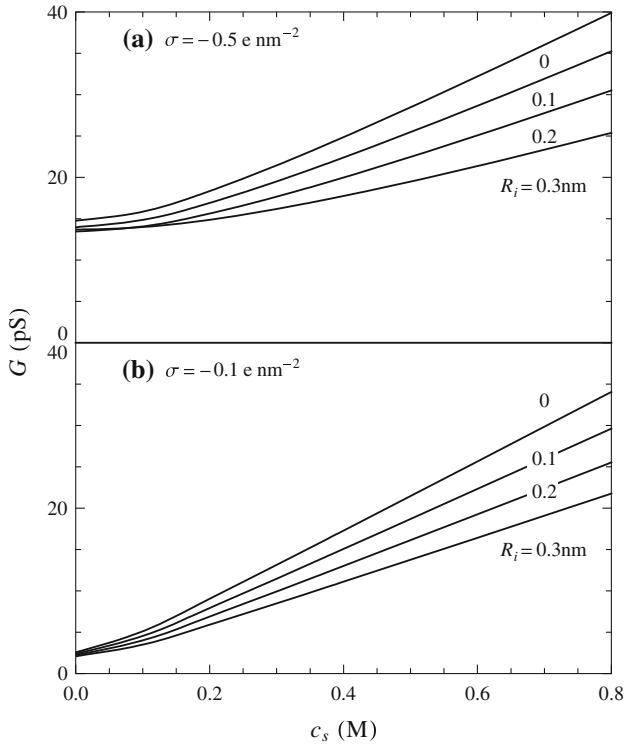

Fig. 3 Electrical conductance G versus the external electrolyte concentration for point and finite-size ions with $R_i = 0.1$, 0.2, and 0.3 nm. The nanopore surface charge density is **a** $\sigma = -0.5$ e/nm^2 and **b** $\sigma = -0.1$ e/nm^2

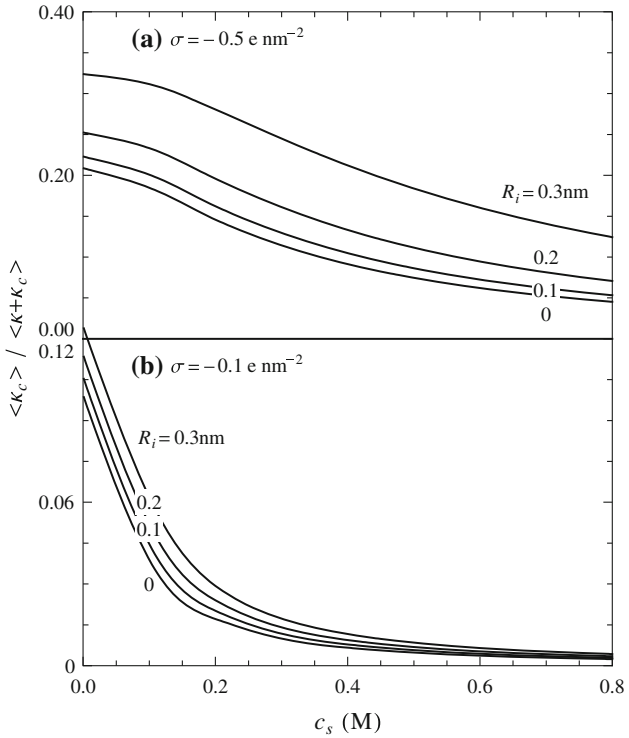

Fig. 4 Relative contribution of electro-osmotic convection to the total electrical conductivity versus the external electrolyte concentration for point ions and finite-size ions with $R_i = 0.1$, 0.2, and 0.3 nm. The nanopore surface charge density is **a** $\sigma = -0.5$ e/nm^2 and **b** $\sigma = -0.1$ e/nm^2

acts on the positively charged pore solution and can be assumed to be laminar under most experimental conditions. Since $\kappa_+ > \kappa_-$ and the convective and migrational flows have the same direction for counter-ions but opposite for co-ions, $\kappa_{c,+}/\kappa_+ = -\kappa_{c,-}/\kappa_- > 0$ (Kontturi et al. 2008), it turns out that the electro-osmosis increases the total conductivity, $\langle \kappa_c \rangle > 0$. The contribution of the electro-osmotic flow to the electrical conductivity is the convective conductivity

$$\langle \kappa_c \rangle \equiv \frac{\varepsilon F}{\eta} \sum_k z_k [\langle c_k \psi \rangle - \langle c_k \rangle \psi^s] = \frac{\varepsilon}{\eta} [\langle \rho_e \psi \rangle - FX\psi^s] \tag{33}$$

This quantity is very small when the electrostatic potential distribution along the radial direction is almost flat. On the contrary, when $\kappa_{D,X} R_p \gg 1$ and $X/c_s > 1$ (which corresponds to high surface charge densities) the large variation of this potential makes $\langle \rho_e \psi \rangle$ to be different from $FX\psi^s$ and $\langle \kappa_c \rangle$ has to be taken into account. In order to make apparent the role of $\langle \kappa_c \rangle$, Fig. 4a, b shows the relative contribution of electro-osmotic convection to the overall conductivity. As shown in Fig. 4b, this contribution accounts for 12% at most of the total conductance for the case of finite size ions and $\sigma = -0.1$ e/nm^2. This result is in agreement with a recent experimental study of the conduction and selectivity of a single nanochannel which concluded that electro-osmosis had a small effect on the total current and could often be neglected for qualitative purposes, especially in the case of long nanopores (Vlassiouk et al. 2008). However, the effect of electro-osmosis can be larger in the case of strongly charged nanopores as shown in Fig. 4a.

Finally, that the $\langle c_+ \rangle + \langle c_- \rangle$ vs. c_s and G vs. c_s curves are concave upwards for finite size and point ions. At very low electrolyte concentrations, there is a conductance saturation that occurs because the co-ion concentration is zero (total co-ion exclusion) while the counter-ion concentration is equal to the (constant) fixed charge concentration inside the nanopore (electroneutrality condition). This saturation is observed experimentally in membranes and nanopores in the low concentration limit (Westermann-Clark and Christoforou 1986; Stein et al. 2004). At moderate electrolyte concentrations, the conductance increase with c_s, in agreement with the experimental observations, due to the increase of $\langle c_+ \rangle + \langle c_- \rangle$ with c_s. At very high concentrations, the calculations predict a linear increase of the conductance with c_s, which is due to our assumptions of constant ionic diffusion coefficients. Experimentally, the G vs. c_s curves are sometimes concave downwards in the high

concentrations range. This is related to a reduction in the effective values for the ionic concentrations and diffusion coefficients inside the pore due to electrostatic interactions between the mobile ions and the pore fixed charges (Mafé et al. 2003 and references therein).

3.3 Counter-ion transport number

When a potential difference is applied between the two external solutions, an electric current flows through the pore. The fraction of current transported by counter-ions, i.e., the (integral) transport number t_+, is a measure of the nanopore selectivity (Cervera et al. 2001a). Figure 3a, b illustrates that the ion size effects increase the nanopore selectivity. If we neglect convection, Eq. 27 simplifies to

$$t_+ \approx \frac{\langle c_+ \rangle}{\langle c_+ \rangle + \langle c_- \rangle} = 1 - \frac{\langle c_- \rangle}{2\langle c_- \rangle + X}, \tag{34}$$

where we have used the electroneutrality condition $\langle c_+ \rangle - \langle c_- \rangle = X$. Equation 34 allows us to explain qualitatively the trends shown in Fig. 5a, b. The transport number t_+ decreases from 1 to 0.5 when increasing the external solution concentration because the average ionic concentrations inside the nanopore also increase with c_s. This is well described by the expression $t_+ = 0.5(1 + [1 + (2c_s/X)^2]^{-1/2})$ derived from the classical Donnan theory for point ions of equal diffusion coefficients. As shown in Fig. 2a, b, ion size effects give enhanced co-ion exclusion and then the transport number t_+ increases with increasing the ionic size.

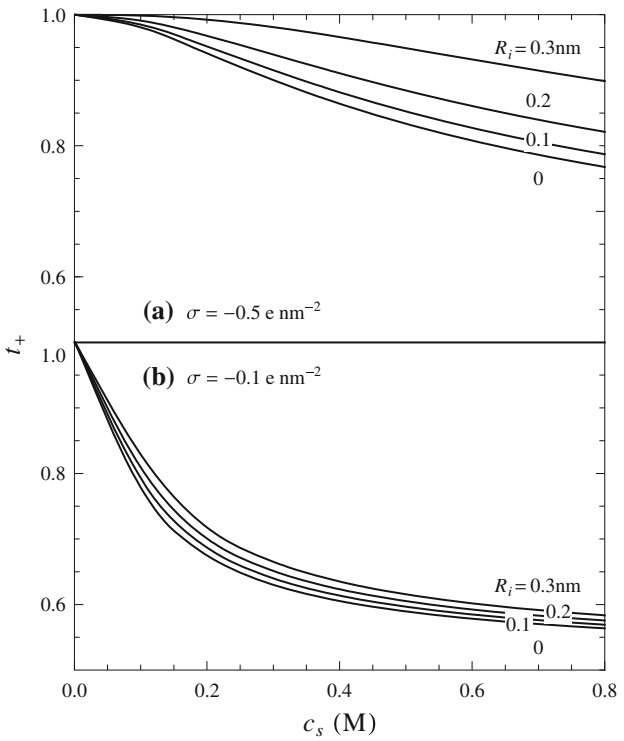

Fig. 5 Integral counter-ion transport number t_+ versus the external electrolyte concentration for point ions and finite-size ions with $R_i = 0.1$, 0.2, and 0.3 nm. The nanopore surface charge density is **a** $\sigma = -0.5$ e/nm^2 and **b** $\sigma = -0.1$ e/nm^2

As shown in Eq. 27, the integral transport number measures the contribution of an ionic species to the electrical conductivity $\kappa + \kappa_c$. To analyze the effect of the convective flow, we note first that $\kappa_+ > \kappa_-$ and that the convective and migrational flows have the same direction for counter-ions but opposite for co-ions, $\kappa_{c,+}/\kappa_+ = -\kappa_{c,-}/\kappa_- > 0$ (Kontturi et al. 2008). Equation 27 then implies that the effect of convection is to enhance the nanopore selectivity. Finally, the effects of ion size and electro-osmotic convection are more noticeable when $c_s \sim X$ because t_+ has fixed limiting values of 1 and 0.5 in the cases of very highly and weakly charged nanopores, regardless of ion size and convection.

3.4 Streaming potential

The streaming potential is the ratio between the resulting potential difference and the applied pressure difference under zero current (Cervera et al. 2001b). Rather surprisingly, the streaming potential [not the streaming current, (van der Heyden et al. 2005)] has not widely employed in the characterization of nanopores in spite of its relative experimental simplicity and considerable use in the case of porous membranes (Kontturi et al. 1994; Huisman et al. 2000; Cervera et al. 2001b; Fievet et al. 2001).

The streaming potential results from the displacement of the space charge present in the nanopore solution induced by the pressure gradient. Since the average value of this charge is constant (due to the electroneutrality condition $\langle c_+ \rangle - \langle c_- \rangle = X$), one might argue that the streaming potential should not depend on the size of the ions and the external concentration. This is not the case, however, because both the space charge and the solution velocity have radial profiles which depends on R_i/R_p and c_s. The streaming potential values can be understood qualitatively from the space charge value at the pore center, where the solution velocity attains its highest value. Increasing the external concentrations allows for a better screening of the fixed charges, which gives a decrease of the space charge at the pore center $\rho_e(0)$ and, therefore, a decrease of the streaming potential as shown in Fig. 6a, b. Figure 6 also shows that the streaming potential increases significantly (about 30–40% in some cases) with the ionic size. This is due to an increase of $\rho_e(0)$ with the ionic size as a consequence of the decrease in the ionic concentrations inside the nanopore with increasing ionic size (see Fig. 2a, b).

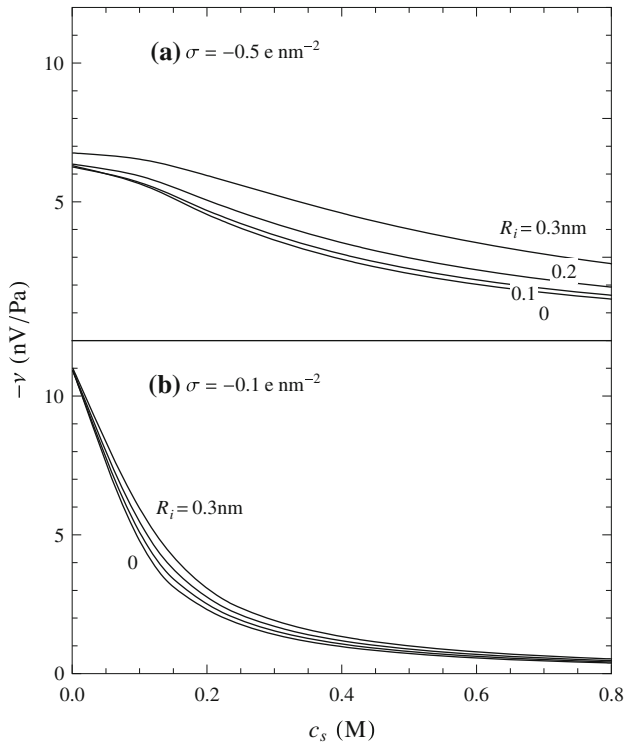

Fig. 6 Streaming potential v versus the external electrolyte concentration for point ions and finite-size ions with $R_i = 0.1$, 0.2, and 0.3 nm. The nanopore surface charge density is **a** $\sigma = -0.5$ e/nm^2 and **b** $\sigma = -0.1$ e/nm^2

3.5 Description of ion size effects using Tsallis' thermostatistics

The ion distribution inside the nanopore is constrained by the finite size. The ions can be in a range of states, from frozen configurations where they are not able to move to diffuse configurations where the traditional P–B approach applies. It has recently been proposed that the ion distribution near macro-ions (Garcia-Morales et al. 2004) and monolayer-protected metal clusters (García-Morales and Mafé 2007; Cervera and Mafé 2008) as well as the charge correlations in free ionic solutions (Varela et al. 2007) can be described using the Tsallis' non-extensive thermostatistics. The effect of the correlations on the ion distribution can be described using the q-exponential distribution, and this leads to a generalized P–B equation in the nanopore solution (García-Morales and Mafé 2007)

$$\frac{1}{r}\frac{\partial}{\partial r}\left(r\frac{\partial \psi}{\partial r}\right) = -\frac{Fc_s}{\varepsilon}\left(e_q^{-f\psi} - e_q^{f\psi}\right), \tag{35}$$

where $e_q^x \equiv [1 + (1-q)x]^{1/(1-q)}$ is the Tsallis q-exponential (Tsallis 1988). The q-parameter is a measure of the restricted motion of the ions due to correlations and structural reasons (García-Morales and Mafé 2007): for $q \to 0$ the ions are "frozen" inside the nanopore, while for

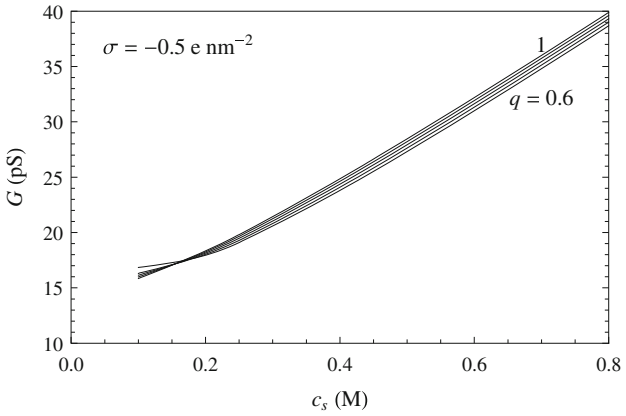

Fig. 7 Electrical conductance G as a function of the external electrolyte concentration for different values of the Tsallis q-parameter ($q = 1$, 0.9, 0.8, 0.7, and 0.6, from top to bottom) and the case of a strongly charged nanopore ($\sigma = -0.5$ e/nm^2)

$q \to 1$ the diffuse P–B equation is regained. The values $q < 1$ reflect the reduction in the phase space available for the ion inside the nanopore solution (Garcia-Morales et al. 2004).

Although the description of finite ion size effects on the transport properties of the nanopore in terms of the partial molar volume v of the ions has provided new physical insights, it seems also interesting to compare the previous results with those obtained from a modification of the P–B equation that introduces the q-parameter instead of v. Figure 7 shows the electrical conductance G as a function of the external electrolyte concentration for the case of a highly charged nanopore ($\sigma = -0.5$ e/nm^2) and different values of the Tsallis q-parameter. For moderate values of q, the behavior of the conductance is the same found for the case of finite size ions: G increases with q because the modification introduced in the P–B equation acts to restrict the movement of the ions. (While the influence of the q-parameter on G appears to be smaller than that of the ion size in Fig. 3, it should be noted that the diffusion coefficients used in Fig. 7 are those of point ions, i.e., no Renkin correction is applied.) For lower values of q, consistently lower conductances G are obtained.

4 Conclusions

We have studied the effect of ion size on the electrical double layer within a charged nanopore with special emphasis on non-equilibrium transport properties such as the streaming potential, the counter-ion transport number, and the electrical conductance. To this end, we have considered generalizations of the P–B approach based on the Bikerman and Tsallis ion distributions. These should be

significant for pore radius of the order of the electrolyte Debye length, which is usually in the nanometer scale. In this limit, the size of the ions could no longer be ignored because they occupy a significant fraction of the pore and, in addition, they would reach unrealistic concentrations at the surface if treated as point charges. The ion size effects on the nanopore characteristics have been discussed as a function of the electrolyte solution concentration for highly and weakly charged nanopores. The ionic selectivity and the streaming potential values increase with ion size. However, the conductance decreases for finite size ions because of the decrease in the average ionic concentrations inside the nanopore and the decreased diffusion coefficients. Even for the case of relatively small inorganic ions at intermediate concentrations, these effects could be significant for a quantitative estimation of nanopore selectivity when the surface charge density is high.

Acknowledgments Support from Ministerio de Ciencia e Innovación, *Programa de Materiales* (MAT2009-07747) and FEDER are acknowledged.

References

Abgrall P, Nguyen NT (2008) Nanofluidic devices and their applications. Anal Chem 80:2326–2341

Aguilella-Arzo M, Cervera J, Ramírez P, Mafé S (2006) Blocking of an ion channel by a highly charged drug: modeling the effects of applied voltage, electrolyte concentration, and drug concentration. Phys Rev E 73:041914-1–041914-6

Alcaraz A, Nestorovich EM, Aguilella-Arzo M, Aguilella VM, Bezrukov SM (2004) Salting out the ionic selectivity of a wide channel: the asymmetry of OmpF. Biophys J 87:943–957

Alcaraz A, Ramírez P, Garcia-Gimenez E, López ML, Andrio A, Aguilella VM (2006) A pH-tunable nanofluidic diode: electrochemical rectification in a reconstituted single ion channel. J Phys Chem B 110:21205–21209

Ali M, Ramírez P, Mafé S, Neumann R, Ensinger W (2009) A pH-tunable nanofluidic diode with a broad range of rectifying properties. ACS Nano 3:603–608

Apel PY, Pretzsch G (1986) Investigation of the radial pore-etching rate in a plastic track detector as a function of the local damage density around the ion path. Nucl Tracks Radiat Meas 11:45–53

Apel PY, Blonskaya IV, Dmitriev SN, Orelovitch OL, Presz A, Sartowska BA (2007) Fabrication of nanopores in polymer foils with surfactant-controlled longitudinal profiles. Nanotechnology 18:305302-1–305302-7

Basu S, Sharma M (1997) An improved space–charge model for flow through charged microporous membranes. J Membr Sci 124: 77–91

Bikerman J (1942) Structure and capacity of the electric double layer. Philos Mag 33:384–397

Bontha JR, Pintauro PN (1994) Water orientation and ion solvation effects during multicomponent salt partitioning in a Nafion cation exchange membrane. Chem Eng Sci 49:3835–3851

Borukhov I, Andelman D, Orland H (1997) Steric effects in electrolytes: a modified Poisson–Boltzmann equation. Phys Rev Lett 79:435–438

Brodowsky H, Strehlow HZ (1959) Zur Struktur der Elektrochemischen Doppelschicht. Z Elektrochem 63:262–269

Buck RP (1984) Kinetics of bulk and interfacial ionic motion: microscopic bases and limits for the Nernst–Planck equation applied to membrane systems. J Membr Sci 17:1–67

Cervera J, Mafé S (2008) Electrical fluctuations in monolayer-protected metal nanoclusters. Chem Phys Lett 451:257–261

Cervera J, Manzanares JA, Mafé S (2001a) Ion size effects on the current efficiency of narrow charged pores. J Membr Sci 191: 179–187

Cervera J, Manzanares JA, Mafé S (2001b) Ion size effects on the streaming potential of narrow charged pores. Phys Chem Chem Phys 3:2493–2496

Cervera J, García-Morales V, Pellicer J (2003) Ion size effects on the electrokinetic flow in nanoporous membranes caused by concentration gradients. J Phys Chem B 107:8300–8309

Cervera J, Schiedt B, Neumann R, Mafé S, Ramírez P (2006) Ionic conduction, rectification, and selectivity in single conical nanopores. J Chem Phys 124:104706-1–104706-9

Chun K-Y, Mafé S, Ramírez P, Stroeve P (2006) Protein transport through gold-coated, charged nanopores: effects of applied voltage. Chem Phys Lett 418:561–564

Cornelius TW, Apel PY, Schiedt B, Trautmann C, Toimil-Molares ME, Karim S, Neumann R (2007) Investigation of nanopore evolution in ion track-etched polycarbonate membranes. Nucl Instrum Methods Phys Res B 265:553–557

Cwirko EH, Carbonell RG (1992) Interpretation of transport coefficients in Nafion using a parallel pore model. J Membr Sci 67: 227–247

Dekker C (2007) Solid-state nanopores. Nat Nanotechnol 2:209–215

Eisenberg RS (1998) Ionic channels in biological membranes: natural nanotubes. Acc Chem Res 31:117–123

Fievet P, Szymczyk A, Labbez C, Aoubiza B, Simon C, Foissy A, Pagetti J (2001) Determining the zeta potential of porous membranes using electrolyte conductivity inside pores. J Colloid Interface Sci 235:383–390

Freise VZ (1952) Zur Theorie der diffusen Doppelschicht. Z Elektrochem 56:822–827

García-Morales V, Mafé S (2007) Monolayer-protected metallic nanoparticles: limitations of the concentric sphere capacitor model. J Phys Chem C 111:7242–7250

Garcia-Morales V, Cervera J, Pellicer J (2004) Coupling theory for counterion distributions based in Tsallis statistics. Physica A 339:482–490

Gracheva ME, Vidal J, Leburton JP (2007) *p–n* semiconductor membrane for electrically tunable ion current rectification and filtering. Nano Lett 7:1717–1722

Griffiths J (2008) The realm of the nanopore. Anal Chem 80:23–27

Grimley TB, Mott NF (1947) The contact between a solid and a liquid electrolyte. Discuss Faraday Soc 1:3–11

Guzmán-García AG, Pintauro PN, Verbrugge MW, Hill RF (1990) Development of a space–charge transport model for ion-exchange membrane. AIChE J 36:1061–1074

Haase R (1969) Thermodynamics of irreversible processes. Addison-Wesley, London

Haubold HG, Vad T, Jungbluth H, Hiller P (2001) Nano-structure of Nafion: a SAXS study. Electrochim Acta 46:1559–1563

Healy K, Schiedt B, Morrison AP (2007) Solid-state nanopore technologies for nanopore-based DNA analysis. Nanomedicine 2:875–897

Heins EA, Siwy Z, Baker LA, Martin CR (2005) Stochastic sensing of a porphyrin molecule in a conically shaped abiotic nanopore. Nano Lett 5:1824–1829

Hille B (2001) Ion channels of excitable membranes. Sinauer Associates, Sunderland

Höltzel A, Tallarek U (2007) Ionic conductance of nanopores in microscale analysis systems: where microfluidics meets nanofluidics. J Sep Sci 30:1398–1419

Hou C-H, Taboada-Serrano P, Yiacoumi S, Tsouris C (2008) Monte Carlo simulation of electrical double-layer formation from mixtures of electrolytes inside nanopores. J Chem Phys 128:044705-1–044705-8

Huisman IH, Prádanos P, Calvo JI, Hernández A (2000) The effect of protein–protein and protein–membrane interactions on membrane fouling in ultrafiltration. J Membr Sci 178:79–90

Jin WQ, Toutianoush A, Tieke B (2005) Size- and charge-selective transport of aromatic compounds across polyelectrolyte multilayer membranes. Appl Surf Sci 246:444–450

Jorne J (2006) Transference number approaching unity in nanocomposite electrolytes. Nano Lett 6:2973–2976

Karginov VA, Nestorovich EM, Moayeri M, Leppla SH, Bezrukov SM (2005) Blocking anthrax lethal toxin at the protective antigen channel by using structure-inspired drug design. Proc Natl Acad Sci 102:15075–15080

Kasianowicz JJ, Brandin E, Branton D, Deamer DW (1996) Characterization of individual polynucleotide molecules using a membrane channel. Proc Natl Acad Sci 93:13770–13773

Kontturi K, Savonen A, Vuoristo M (1994) Study of adsorption and ion exchange properties of some porous membranes. Acta Chem Scand 48:1–11

Kontturi K, Murtomäki L, Manzanares JA (2008) Ionic transport processes in electrochemistry and membrane science. Oxford University Press, Oxford

Ku JR, Lai SM, Ileri N, Ramírez P, Mafé S, Stroeve P (2007) pH and ionic strength effects on aminoacid transport through Au-nanotubule membranes charged with self-assembled monolayers. J Phys Chem C 111:2965–2973

Lebedev K, Mafé S, Stroeve P (2005) Modeling electrochemical deposition inside nanotubes to obtain metal–semiconductor multiscale nanocables or conical nanopores. J Phys Chem B 109:14523–14528

Lee S, Zhang YH, White HS, Harrell CC, Martin CR (2004) Electrophoretic capture and detection of nanoparticles at the opening of a membrane pore using scanning electrochemical microscopy. Anal Chem 76:6108–6115

Levine S, Bell GM (1960) Theory of a modified Poisson–Boltzmann equation I. The volume effect of hydrated ions. J Phys Chem 64:1188–1195

Liu S, Pu Q, Gao L, Korzeniewski C, Matzke C (2005) From nanochannel-induced proton conduction enhancement to a nanochannel-based fuel cell. Nano Lett 5:1389–1393

Mafé S, Manzanares JA, Pellicer J (1990) On the introduction of the pore wall charge in the space–charge model for microporous membranes. J Membr Sci 51:161–168

Mafé S, Manzanares JA, Ramírez P (2003) Modelling of surface vs. bulk ionic conductivity in fixed charge membranes. Phys Chem Chem Phys 5:376–383

Manzanares JA, Mafé S, Pellicer J (1991) Pore conductivity and streaming potential in charged capillary tubes with concentration dependent pore wall charge. J Non-Equilib Thermodyn 16: 255–265

Martin CR, Siwy ZS (2007) Learning nature's way: biosensing with synthetic nanopores. Science 317:331–332

Miedema H, Vrouenraets M, Wierenga J, Meijberg W, Robillard G, Eisenberg B (2007) A biological porin engineered into a molecular, nanofluidic diode. Nano Lett 7:2886–2891

Muthukumar M, Kong CY (2006) Simulation of polymer translocation through protein channels. Proc Natl Acad Sci 103:5273–5278

Nishizawa M, Menon VP, Martin CR (1995) Metal nanotubule membranes with electrochemically switchable ion-transport selectivity. Science 268:700–702

Pade V, Stavchansky S (1997) Estimation of the relative contribution of the transcellular and paracellular pathway to the transport of passively absorbed drugs in the Caco-2 cell culture model. Pharm Res 14:1210–1215

Paunov VN, Binks BP (1999) Analytical expression for the electrostatic disjoining pressure taking into account the excluded volume of the hydrated ions between charged interface in electrolyte. Langmuir 15:2015–2021

Petrossian L, Wilk SJ, Joshi P, Goodnick SM, Thornton TJ (2008) Demonstration of Coulter counting through a cylindrical solid state nanopore. J Phys Conf Ser 109:012028-1–012028-4

Qiao R, Aluru NR (2005) Atomistic simulation of KCl transport in charged silicon nanochannels: interfacial effects. Colloids Surf A 267:103–109

Ramírez P, Mafé S, Aguilella VM, Alcaraz A (2003a) Synthetic nanopores with fixed charges: an electrodiffusion model for ionic transport. Phys Rev E 68:011910-1–011910-8

Ramírez P, Mafé S, Alcaraz A, Cervera J (2003b) Modeling of pH-switchable ion transport and selectivity in nanopore membranes with fixed charges. J Phys Chem B 107:13178–13187

Ramírez P, Gómez V, Cervera J, Schiedt B, Mafé S (2007) Ion transport and selectivity in nanopores with spatially inhomogeneous fixed charge distributions. J Chem Phys 126:194703-1–194703-9

Ramírez P, Apel PY, Cervera J, Mafé S (2008) Pore structure and function of synthetic nanopores with fixed charges: tip shape and rectification properties. Nanotechnology 19:315707-1–315707-12

Renkin EM (1954) Filtration, diffusion, and molecular sieving through porous cellulose membranes. J Gen Physiol 38:225–243

Robertson JWF, Rodrigues CG, Stanford VM, Rubinson KA, Krasilnikov OV, Kasianowicz JJ (2007) Single-molecule mass spectrometry in solution using a solitary nanopore. Proc Natl Acad Sci 104:8207–8211

Schoch RB, Han J, Renaud P (2008) Transport phenomena in nanofluidics. Rev Mod Phys 80:839–883

Sexton LT, Horne LP, Martin CR (2007a) Developing synthetic conical nanopores for biosensing applications. Mol BioSyst 3:667–685

Sexton LT, Horne LP, Sherrill SA, Bishop GW, Baker LA, Martin CR (2007b) Resistive-pulse studies of proteins and protein/antibody complexes using a conical nanotube sensor. J Am Chem Soc 129:13144–13152

Siwy Z, Fulinski A (2002) Fabrication of a synthetic nanopore ion pump. Phys Rev Lett 89:198103-1–198103-4

Sparnaay MJ (1972) The electrical double layer. Pergamon Press, Oxford

Spohr R (2005) Status of ion track technology—prospects of single tracks. Radiat Meas 40:191–202

Stein D, Kruithof M, Dekker C (2004) Surface-charge-governed ion transport in nanofluidic channels. Phys Rev Lett 93:035901-1–035901-4

Striemer CC, Gaborski TR, McGrath JL, Fauchet PM (2007) Charge- and size-based separation of macromolecules using ultrathin silicon membranes. Nature 445:749–753

Tabard-Cossa V, Trivedi D, Wiggin M, Jetha NN, Marziali A (2007) Noise analysis and reduction in solid-state nanopores. Nanotechnology 18:305505-1–305505-6

Tsallis CJ (1988) Possible generalization of Boltzmann–Gibbs statistics. J Stat Phys 52:479–487

Umehara S, Pourm N, Webb CD, Davis RW, Yasuda K, Karhanek M (2006) Current rectification with poly-l-lysine-coated quartz nanopipettes. Nano Lett 6:2486–2492

van der Heyden FHJ, Stein D, Dekker C (2005) Streaming currents in a single nanofluidic channel. Phys Rev Lett 95:116104-1–116104-4

Varela LM, Carrete J, Muñoz-Solá R, Rodríguez JR, Gallego J (2007) Nonextensive statistical mechanics of ionic solutions. Phys Lett A 370:405–412

Vlassiouk I, Siwy Z (2007) Nanofluidic diode. Nano Lett 7:552–556
Vlassiouk I, Smirnov S, Siwy Z (2008) Ionic selectivity of single nanochannels. Nano Lett 8:1978–1985
Westermann-Clark GB, Christoforou CC (1986) The exclusion-diffusion potential in charged porous membranes. J Electroanal Chem 198:213–231
Wharton JE, Jin P, Sexton LT, Horne LP, Sherrill SA, Mino WK, Martin CR (2007) A method for reproducibly preparing synthetic nanopores for resistive-pulse biosensors. Small 3:1424–1430
Wicke E, Eigen MZ (1953) Thermodynamische Eigenschaften konzentrierterer wäbriger Elektrolytlösungen. Z Elektrochem 57:319–390
Yeh I-C, Hummer G (2004) Nucleic acid transport through carbon nanotube membranes. Proc Natl Acad Sci 101:12177–12182
Zhang YH, Zhang B, White HS (2006) Electrochemistry of nanopore electrodes in low ionic strength solutions. J Phys Chem B 110:1768–1774
Zhao Q, Sigalov G, Dimitrov V, Dorvel B, Mirsaidov U, Sligar S, Aksimentiev A, Timp G (2007) Detecting SNPs using a synthetic nanopore. Nano Lett 7:1680–1685